Buckling instability of Web Plastifying Dampers: analytical and numerical approach

E. Oliver-Saiz, A. Benavent-Climent, A.L.- Ramírez-Márquez
Department of Structural Mechanics and Hydraulic Engineering. University of Granada, Spain.

SUMMARY:
This paper describes a numerical study on the instability of a brace-type seismic damper based on the out-of-plane yielding of the web of wide-flange steel sections (Web Plastifying Damper, WPD). The damper is intended to be installed in a framed structure as a standard diagonal brace. Under lateral forces, the damper is subjected to high axial forces, therefore its buckling instability is a matter of concern. Several finite element models representing WPDs with different axial stiffness and various geometries of their components were developed and analyzed taking into account both material and geometrical nonlinearities. The influence of several parameters defining the WPD in the load-displacement curve was examined. Furthermore, a simplified model to predict the buckling load is proposed.

Keywords: Dampers, Buckling, Hysteretic behaviour, Bracing member, Post-buckling strength.

1. INTRODUCTION

Hysteretic dampers are often considered one of the most effective and inexpensive passive seismic techniques. The dampers can de designed so that most of the energy input by the earthquake is dissipated in specially prepared components of the structure (the dampers) thus limiting the damage on the main frame (Martinez-Rueda, 2002). Therefore, the energy dissipation demand on critical components of the main structure can be drastically reduced by transferring the energy dissipation demand to these passive energy dissipation devices (Symans et al., 2008). In the case of metallic dampers, energy is dissipated by the yielding of ductile metals such as steel, materials that are easy and reliable to characterize.

A recently proposed type of hysteretic damper WPD (*Web Plastifying Damper*) is analysed in this paper. It has the form of a conventional brace and it is based on yielding the web of short segments of wide-flange or I-shape steel sections under out-of-plane bending (Benavent-Climent et al., 2010). Since it has the form of a conventional brace and it is intended to be installed in a framed structure as a standard diagonal bar, it will be subjected to high axial forces, so its buckling instability is a matter of concern. Under high compressive loads, conventional braces tend to buckle producing a sudden reduction of their strength (Fell et al., 2009), (Tremblay, 2002). A possible solution consists of restraining buckling of the brace, so that it exhibits the same behaviour both in tension and compression (Xie, 2005), such as *buckling-restrained braces* (BRBs).

2. WPD BRACE-DAMPER CONFIGURATION

2.1. WPD device description (*Web Plastifying Damper*)

As mentioned before, the device is constructed by assembling several short length segments of wide-flange or I-shaped sections, which constitute the energy-dissipating device, and other auxiliary steel bars that remain in elastic range, as shown in Fig.1. The assemblage is arranged in such a way that

when the brace damper is subjected to forced deformations in the axial direction, the web of the wide-flange or I-shape section undergoes out-of-plane flexural deformations (Benavent-Climent et al., 2010), and auxiliary steel bars bear high compressive loads.

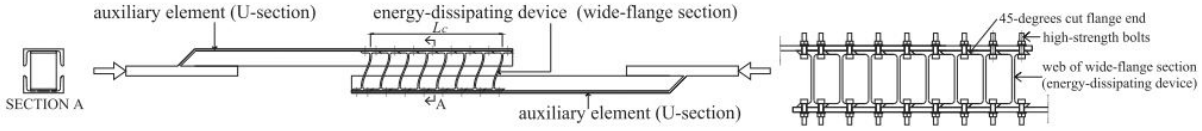

Figure 1: WPD device(Benavent-Climent et al., 2010)

2.2. Configurations of WPD damper

Several ways of arranging the short length segments of wide-flange or I-shaped sections to form the WPD damper were examined, obtaining different post-buckling behaviours. The first configuration, labelled as type A, is shown in Fig.2 and it consists in mounting one row of segments of I-sections in series with two U-shape steel profiles. In the second and third configurations, referred to as types B and C, the segments of I-shaped sections are arranged in two rows as shown in Figs. 3 and 4 respectively. The only formal difference between types B and C is the shape of the auxiliary elements used. All types of WPD damper configurations considered were designed taking into account architectonical considerations, such as the possibility of keep them into the exterior walls or partitions, by limiting their maximum width to 40 cm. In addition, auxiliary elements were designed according to Spanish Standards to avoid buckling.

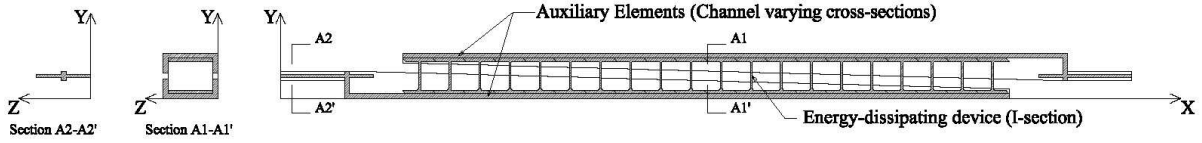

Figure 2.WPD damper configurationA

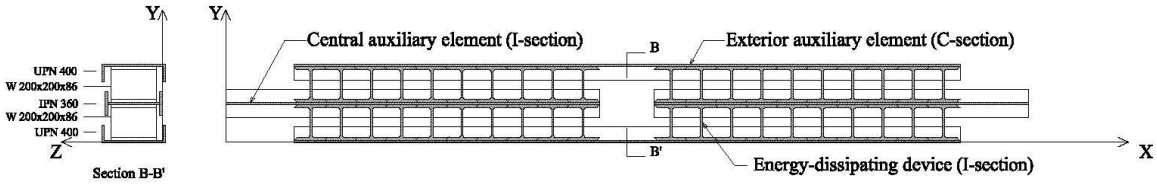

Figure3.WPD damper configuration B

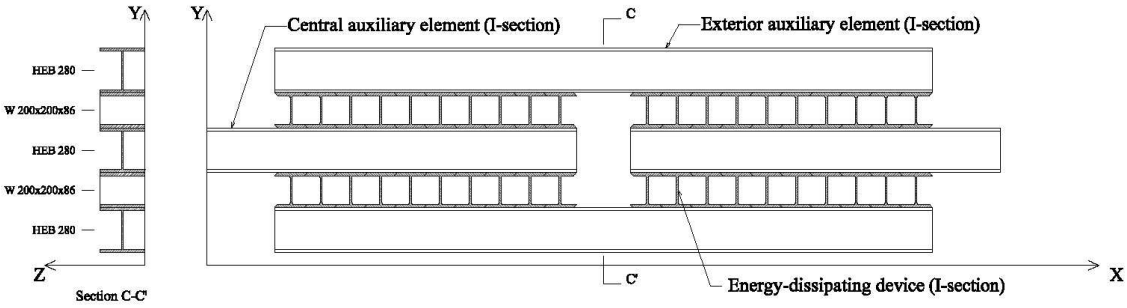

Figure 4.WPD damper configuration C

The axial stiffness and yield strength of the three configurations of dampers (A, B and C) described above are summarized in Table 2.1.

Table 2.1. Axial stiffness, axial strength and yields displacement of WPD dampers

Configuration A	*Configurations B and C*
$Q_{TY} = n\,q_y$	$Q_{TY} = \frac{n}{2} q_y$
$\delta_{TY} = \delta_y$	$\delta_{TY} = 2\,\delta_y$
$k_e = \frac{q_y}{\delta_y}; \qquad K_{TE} = \frac{Q_{TY}}{\delta_{TY}} = \frac{n\,q_y}{\delta_y} = n\,k_e$	$k_e = \frac{q_y}{\delta_y}; \qquad K_{TE} = \frac{Q_{TY}}{\delta_{TY}} = \frac{\frac{n}{2} q_y}{2\,\delta_y} = \frac{n}{4} k_e$

Where, Q_{Ty} and δ_{TY} are the total axial yield force and axial yield displacement of the damper; q_y and δ_y are the yield shear force and yield displacement of a single I-section segment; K_e is the total elastic stiffness of the damper; k_e is the elastic stiffness of a single I-section steel segment; and n is the number of I-section steel segments that form the WPD damper. For the purposes of this study, three WPD dampers of type A, B and C were designed for the same yield load Q_{Ty}=1000kN. In addition, the same type and dimensions for the I-section segments were used (W200×200×86), each of which had a yield load q_y=50 kN. The formulae for q_y can be found elsewhere (Benavent-Climent et al., 2010).

3. NUMERICAL TESTS

In order to study the buckling behaviour of the different configurations, Finite Element Models (FEM) were developed by using the software ANSYS v.12.1. Nonlinear static analyses were carried out taking into account both material and geometrical nonlinearities. The numerical models included the energy dissipating devices (i.e. the I-section steel segments) and the auxiliary elements. The nonlinear behaviour of the energy dissipating devices was calibrated using experimental dataavailable from previous experiments (Benavent-Climent et al., 2010). Details on this calibration can be found elsewere (Oliver-Saiz and Benavent-Climent, 2011). The numerical models of the complete configurations (i.e. the energy dissipating devices and the auxiliary elements) were subjected to imposed displacements *UX*, applied in the axial direction of the WPD damper. The auxiliary elements were defined with an elastic material (with elastic modulus E=210000N/mm2 and Poisson's ratio μ=0.3), while energy-dissipating devices were defined using a bilinear stress-strain model with yield strength $\sigma_y = 340$ MPa and ultimate strength $\sigma_u = 441$ MPa. These values were obtained in previous tests (Benavent-Climent et al., 2010). Figure 5 shows the load-displacement curves obtained for each configuration (Oliver-Saiz and Benavent-Climent, 2011), and it can be seen that the buckling of WPD dampers develops in a stable way, unlike conventional braces, which buckling always implies a sudden decrease of axial strength. In case of configuration B, it is seen in figure 5 that when the bending stiffness of the exterior auxiliary element (see Figs. 3 and 4) is low the performance of the WPD damper is better than when it is high, because the plastic branch of the axial load-displacement curve is flatter. To further investigate the effect of the bending stiffness k_b of the exterior auxiliary element, additional numerical tests were conducted in which different values of k_b were adopted. For convenience, k_b was expressed as a fraction of the plastic stiffness k_{p1} of the energy-dissipating devices (I-section steel segment) by means of a parameter γ defined by $\gamma=k_b/k_{p1}$. It is worth noting that all WPD damper configurations used a similar energy dissipating device (W200x200x86), therefore k_{p1} had the same value in all numerical models. Fig. 6 shows the axial load-displacement curve obtained for configurations A and B.

As can it can be observed in Fig. 6, the post-yield behaviour is different in compression and in tension. In compression, the load increases up to a point where bucking occurs and the curve flattens. On the contrary, in tension, since buckling does not occur, the axial load keeps increasing due to strain hardening and second order effects. Further, the maximum axial load developed in compression by the WPD damper increases with γ. It is worth emphasizing that in contrast to conventional braces in compression, after buckling the axial strength of the WPD damper does not decrease suddenly but maintains an approximate horizontal slope, with is a desirable behaviour.

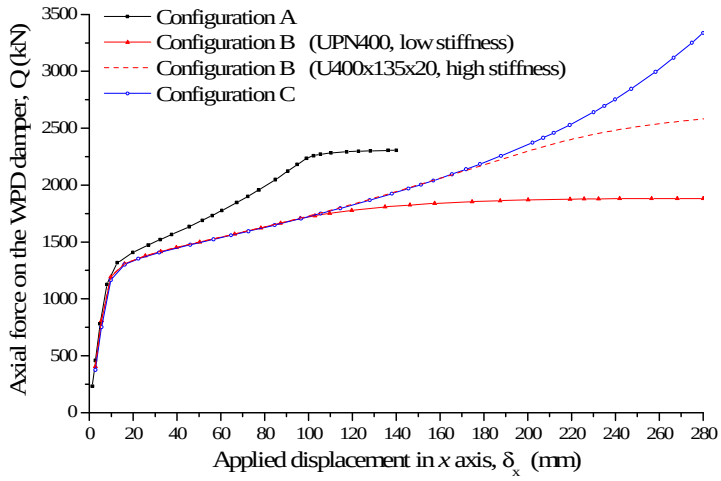

Figure 5. Load-displacement curves obtained for each configuration (Oliver-Saiz and Benavent-Climent, 2011)

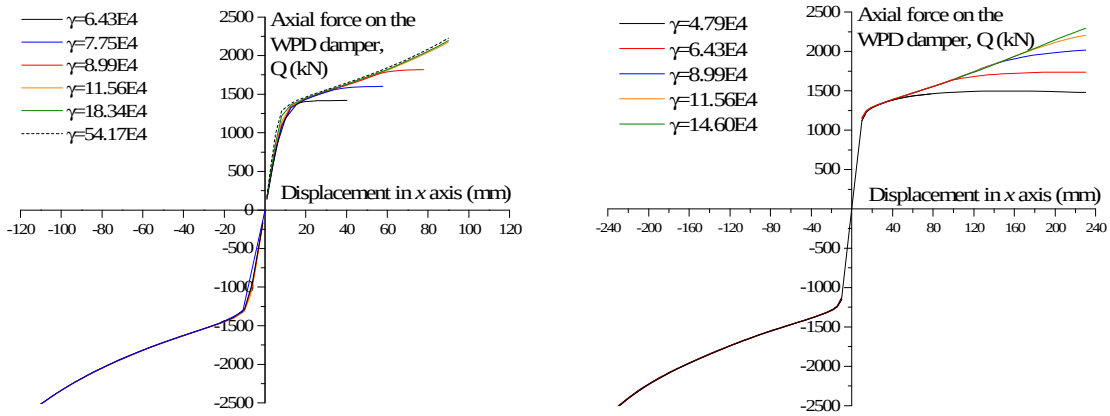

a) Configuration A b) Configuration B

Figure 6. Axial load displacement curves for different values of$\gamma=k_b/k_{p1}$.

The FEM analyses conducted to clarify the influence of parameter γ were also useful to study the deformation pattern of the WPD dampers, which is shown in figures 7 to 8. As observed in Fig. 7 and, especially, in Fig.8, before buckling, all energy-dissipating devices (i.e. I-section steel segments) deform equally and in the same direction, as in tension. However, after buckling, Fig. 8 shows that the lower row of energy-dissipating devices increases its compressive deformation, while the upper row reduces its deformation (unloading). This behavior is used in next section to develop an analytical model to predict the critical buckling load and post buckling behavior.

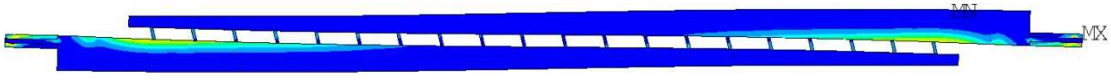

a) UX= +40 mm

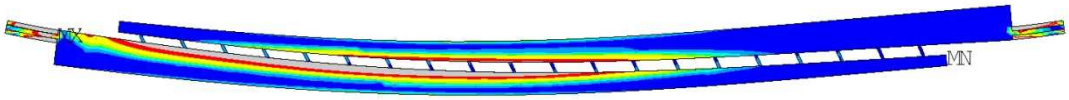

b) UX= +200 mm

c) UX= -71 mm

Figure 7. Deformation patterns and Von Mises stress (N/m^2) in WPD damper configuration A: a) compression before buckling; b) in compression after buckling; c) in tension

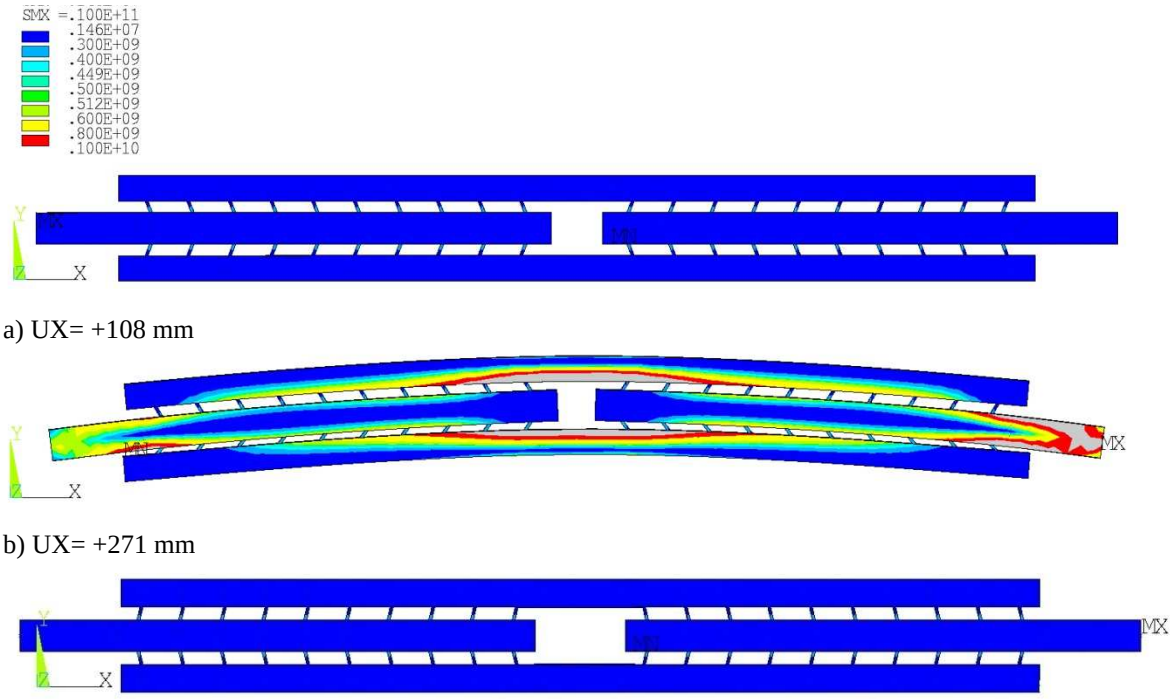

a) UX= +108 mm

b) UX= +271 mm

c) UX= -71 mm

Figure 8. Deformation patterns and Von Mises stress (N/m^2) in WPD damper configuration C: a) compression before buckling; b) in compression after buckling; c) in tension

4. ANALITICAL APPROACHFOR DAMPER CONFIGURATIONS B AND C

In this section, an attempt is made to obtain a simple analytical expression for estimating the buckling load of the WPD type damper, that follows previous work (Benavent-Climent, 1998). To this end, the inelastic buckling column theories of Engesser and Shanley are used (Engesser, 1889, Shanley, 1947). To this end the WPD damper is idealized as shown in Fig. 9. The I-section steel segments (energy dissipating devices) are replaced by shear springs and pin-ended truss elements. The shear springs represents the out-of-plane shear stiffness of the web of the energy dissipating devices. As shown in Fig. 9 each shear spring represents *n/4* energy dissipating devices, where *n* is the total number energy dissipating devices arranged in the device. The load-displacement curve of each energy dissipating device is idealized here as a bilinear curve defined by an initial elastic stiffness k_e and a plastic stiffness k_p which value is taken as k_p =1/30 k_e following past research (Benavent-Climent et al., 2010). By using the model shown in Fig. 9, the critical buckling load can be predicted assuming thatthe WPD damper is first axially compressed without buckling untilthe yielding load Q_{Ty} is reached (Fig. 9.b). Beyond this point (i.e. after yielding), the WPD damper is assumed to buckle experiencing a lateral displacement characterized by the rotation angle θ (Fig. 9.c). The final total shear deformation of the shear springs (Fig. 9.d) is the sum of that induced by the initial (i.e. before buckling) axial deformation of the WPD damper (Fig.9.b) δ_o=x_o/2, plus the additional deformation caused by the lateral displacement of the WPD damper due to buckling $\Delta\delta_1$ or $\Delta\delta_2$ (Fig. 9.c). It is worth emphasizing that shear springs at one side of the axis of the WPD damper increase their shear deformation after buckling, while the shear springs of the other side reduce the initial deformation. The critical buckling load can be determined by equating internal and external bending moments as follows.

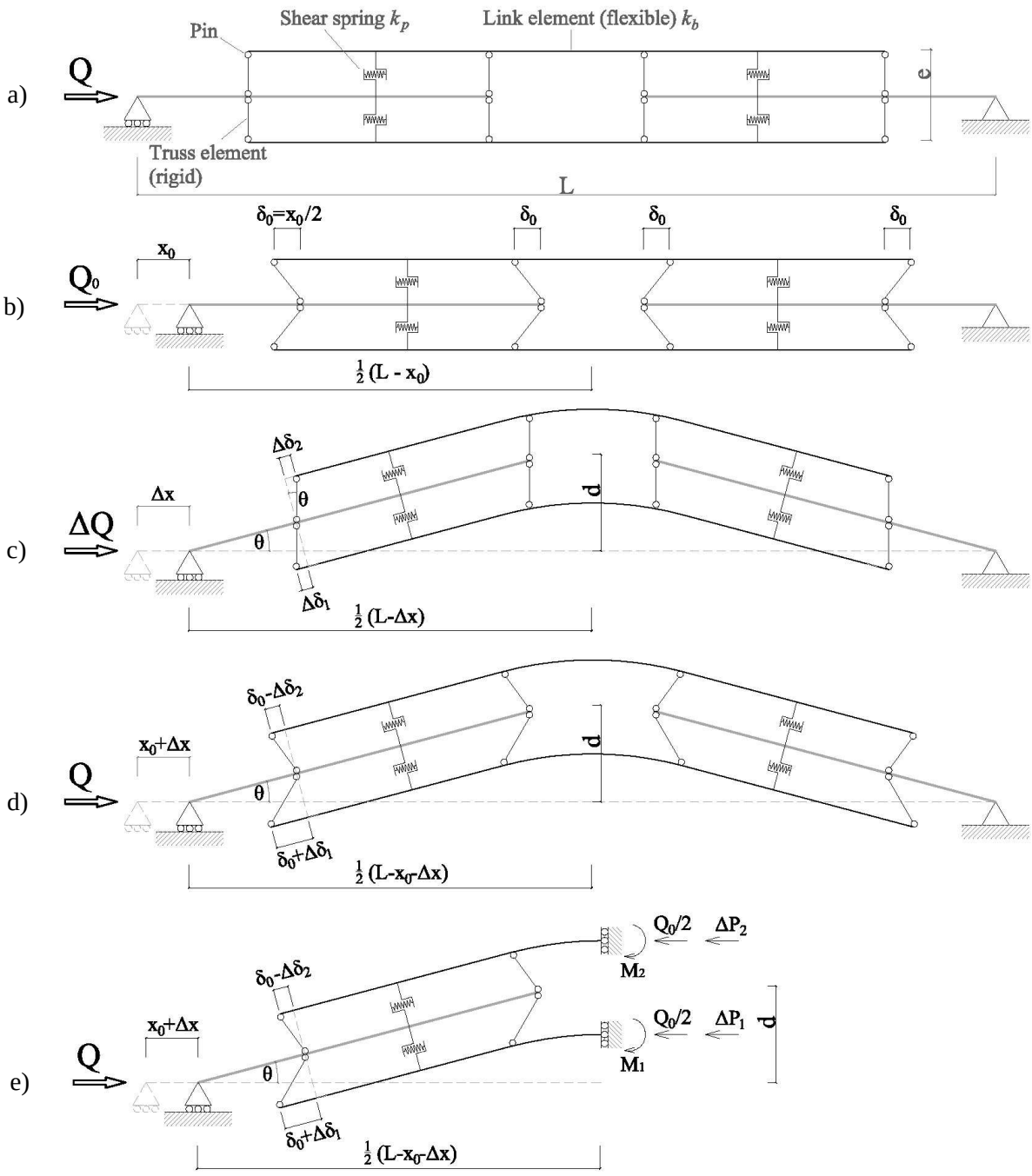

Figure 9. Deformation pattern of the WPD damper: a) model for predicting buckling of the WPD damper; b) deformation pattern before buckling; c) deform pattern due to lateral displacement; d) deform pattern after buckling; e) Free body diagram

The lateral deflection, *d*, of the WPD damper can be approximated as follows:

$$d = \frac{1}{2}\tan\theta\,(L-\Delta x) = \frac{1}{2\,e}(\Delta\delta_1+\Delta\delta_2)(L-\Delta x) \tag{4.1}$$

where L is the total length of the damper; Δx is the increment of axial displacement associated with buckling (Fig.9); θ is the angle between the axis of the WPD damper and the horizontal shown in Fig. 9; $\Delta\delta_1$ and $\Delta\delta_2$ are the increments of deformation on the shear springs at each side of the axis of the WPD damper caused by buckling. The external bending momentM_e is:

$$M_e = Qd = \frac{Q}{2\,e}(\Delta\delta_1+\Delta\delta_2)(L-\Delta x) \tag{4.2}$$

Where Q=Q_t+ΔQ is the load applied at the axis of the WPD damper when buckling occurs. The increment of force on the shear springs ΔP_1 and ΔP_2, are:

$$\Delta P_1 = k_{p1}\Delta\delta_1 \qquad \Delta P_2 = k_{p2}\Delta\delta_2 \tag{4.3}$$

Where k_{p1} and k_{p2} are the stiffness of the shear strings. The bending moments exerted by the exterior auxiliary elements at the central section, M_1 and M_2 are

$$M_1 = k_{b1}\theta \qquad M_2 = k_{b2}\,\theta \tag{4.4}$$

Where k_{b1} and k_{b2} are the bending stiffnesses of the external auxiliary elements given by:

$$k_{b1} = k_{b2} = \frac{EI}{L_{aux}}\theta = k_b \tag{4.5}$$

Here L_{aux} is taken L_{aux}=L/2. The internal bending moment $M_i$about the hinge is

$$M_i = \frac{e}{2}\left(k_{p1}\Delta\delta_1 + k_{p2}\Delta\delta_2\right) + 2\,k_b \tag{4.6}$$

Equating internal and external bending moments

$$Q\,d = \frac{e}{2}\left(k_{p1}\Delta\delta_1 + k_{p2}\Delta\delta_2\right) + 2\,k_b\,\theta \tag{4.7}$$

4.1.1. Tangent modulus critical buckling load

In order to estimate a lower bound of the critical buckling load of the WPD damper, and following the tangent modulus approach of Engesser (Engesser, 1889), it is assumed that immediately before buckling, the stiffness of the shear springs that represent the I-section steel segments k_{p1}, k_{p2} have the same value $k_{p1} = k_{p2} = k_p$, therefore:

$$Q_t d = \frac{e}{2}k_p(\Delta\delta_1 + \Delta\delta_2) + 2\,k_b\,\theta \tag{4.8}$$

Substituting Eqn. 4.1 and $\theta = \frac{(\Delta\delta_1+\Delta\delta_2)}{e}$ in Eq. (4.8), and taking $x_0 \cong 0$ for simplicity gives:

$$Q_t = \frac{e^2}{L}k_p + \frac{4}{L}k_b \tag{4.9}$$

4.1.2. Post-buckling expression

In order to obtain an expression that relates the axial load applied on the WPD damper and the axial displacement, the variables $\Delta\delta_1$ and $\Delta\delta_2$ must be eliminated in above equations. To this end, a new expression is developed next by following Shanley's theory. It is assumed that after buckling (i.e. once the tangent modulus critical buckling load Q_t is attained), the axial force on the WPD damper increases an amount ΔQ, that is the difference between loads ΔP_1 and ΔP_2.

$$Q = Q_t + \Delta Q = Q_t + \Delta P_1 - \Delta P_2 = Q_t + k_{p1}\Delta\delta_1 - k_{p2}\Delta\delta_2 \tag{4.10}$$

Substituting Eqn. 4.9in Eqn. 4.10, gives:

$$Q = \frac{e^2}{L}k_p + \frac{4}{L}k_b + k_{p1}\Delta\delta_1 - k_{p2}\Delta\delta_2 \tag{4.11}$$

Solving Q in Eqn. 4.7 and equating withEq. 4.11 gives:

$$Q = \frac{e}{2d}\left(k_{p1}\Delta\delta_1 + k_{p2}\Delta\delta_2\right) + \frac{2}{d}k_b\,\theta = \frac{e^2}{L}k_p + \frac{4}{L}k_b + k_{p1}\Delta\delta_1 - k_{p2}\Delta\delta_2 \tag{4.12}$$

Substituting $\theta = \frac{(\Delta\delta_1+\Delta\delta_2)}{e}$ gives:

$$\frac{e}{2d}\left(k_{p1}\Delta\delta_1 + k_{p2}\Delta\delta_2\right) + \frac{2}{d}k_b\frac{(\Delta\delta_1+\Delta\delta_2)}{e} = \frac{e^2}{L}k_p + \frac{4}{L}k_b + k_{p1}\Delta\delta_1 - k_{p2}\Delta\delta_2 \tag{4.13}$$

Taking into account the Eqn. 4.1, the variable δ_1 can be expressed as follows:

$$\Delta\delta_1 = \frac{2de}{(L-\Delta x)} - \Delta\delta_2 \tag{4.14}$$

Substituting Eqn. 4.14 into Eqn. 4.13, and solving for $\Delta\delta_2$ gives:

$$\Delta\delta_2 = \frac{-4\,k_b + k_{p1}(2de-e^2)}{(L-\Delta x)\left(k_{p2}\left(1+\frac{e}{2d}\right)+k_{p1}\left(1-\frac{e}{2d}\right)\right)} + \frac{e^2k_p+4k_b}{L\left(k_{p2}\left(1+\frac{e}{2d}\right)+k_{p1}\left(1-\frac{e}{2d}\right)\right)} \tag{4.16}$$

Susbtituting Eqs. (4.14) and (4.16) in Eqn. 4.7, and noting that $k_{p1} = k_p$ gives:

$$Q = \frac{e}{2d}\left(k_{p1}\left(\frac{2de}{(L-\Delta x)} - \frac{-4\,k_b + k_{p1}(2de-e^2)}{(L-\Delta x)\left(k_{p2}\left(1+\frac{e}{2d}\right)+k_{p1}\left(1-\frac{e}{2d}\right)\right)} - \frac{e^2k_{p1}+4k_b}{L\left(k_{p2}\left(1+\frac{e}{2d}\right)+k_{p1}\left(1-\frac{e}{2d}\right)\right)}\right) + k_{p2}\left(\frac{-4\,k_b + k_{p1}(2de-e^2)}{(L-\Delta x)\left(k_{p2}\left(1+\frac{e}{2d}\right)+k_{p1}\left(1-\frac{e}{2d}\right)\right)} + \frac{e^2k_{p1}+4k_b}{L\left(k_{p2}\left(1+\frac{e}{2d}\right)+k_{p1}\left(1-\frac{e}{2d}\right)\right)}\right)\right) + k_b\frac{4}{(L-\Delta x)} \tag{4.18}$$

The relation between *d* and Δ*x* can be established as follows:

$$d = \sqrt{\frac{L^2-(L-\Delta x)^2}{4}} \tag{4.19}$$

Eq. (4.18) can be simplified assuming that $(L-\Delta x) \cong L$, which leads to the following expression provides results similar to Eq. (4.19):

$$Q = \frac{k_{p1}e^2}{L}\left(1 + \frac{1}{\left(k_{p2}\left(1+\frac{e}{2d}\right)+k_{p1}\left(1-\frac{e}{2d}\right)\right)}\left(k_{p2}-k_{p1}\right)\right) + k_b\frac{4}{L} \tag{4. 21}$$

Figure 11 represents the ratio $R=Q/Q_t$ against the parameter γ defined in previous sections as the relation between k_{p1} and k_b. It can be seen in Fig. 12, R decreases as γ increases.

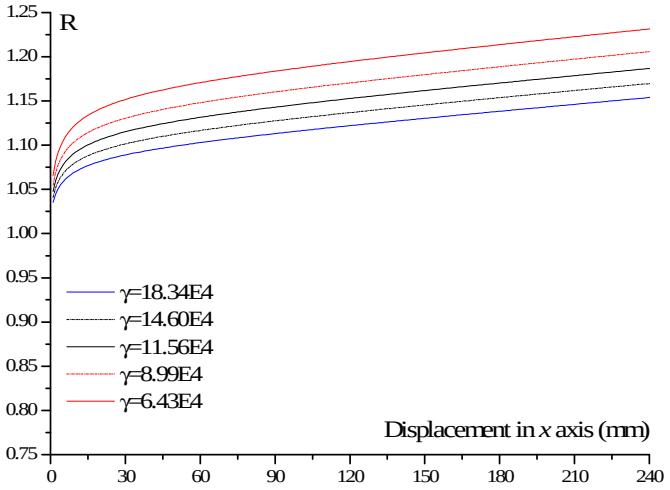

Figure 11. Coefficient *R* is plotted for several stiffness relations

5. COMPARISON BETWEEN NUMERICAL TESTS AND ANALYTICAL APPROACH

Fig. 12 compares the axial load-displacement curves for different values of $\gamma=k_b/k_{p1}$ obtained in the numerical tests, with the curve provided by Eqn. 4.21. It can be observed that the buckling behaviour of the damper can be reasonably well approximated with the analytical expression proposed in section 4.

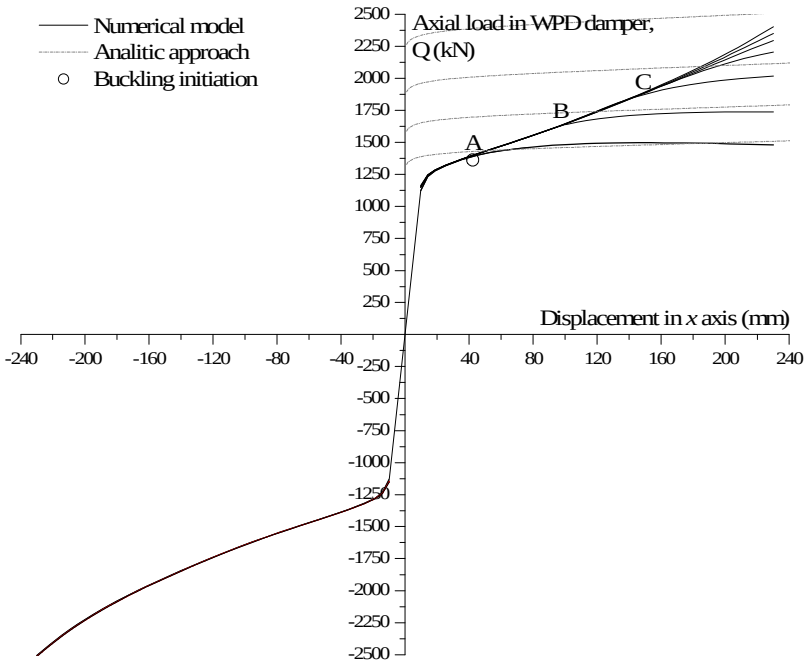

Figure 23. Numerical data is plotted with analytical expression for different stiffness relations.

6. CONCLUSIONS

This paper investigated the buckling instability of a new type of hysteretic damper, referred to as WPD damper, that is intended to be installed in a frame as a conventional brace. In contrast to conventional members subjected to compressive loads, this paper shows that theWPD brace damper exhibits a stable post-buckling behaviour and that the critical buckling load can be easily predicted using a simple analytical model.

7. ACKNOWLEDGEMENTS

This research was funded by the local government of Spain, *Consejería de Innovación, Ciencia y Tecnología* through the project number P07-TEP-02610 and by the European Union (*Fonds Européen de Development Regional*).

8. BIBLIOGRAPHY

Ansys Inc (1994) *ANSYS user's manual for revision 5.1,* Houston, ANSYS.

Benavent-Climent, A. (1998) Seismic design of structures by using brace-type hysteretic dampers. Universidad de Tokio (Japón)

Benavent-Climent, A., Morillas, L. & Vico, J. M. (2010) A study on using wide-flange section web under out-of-plane flexure for passive energy dissipation. *Earthquake Engineering & Structural Dynamics***,** 473-490.

Engesser, F. (1889) Ueber die Knickfestigkeit gerader stäbe. *Zeitschrift für Arhitektur und Ingenieurwesen,* 35**,** 455-462.

Fell, B. V., Kanvinde, A. M., Deierlein, G. G. & Myers, A. T. (2009) Experimental Investigation of Inelastic Cyclic Buckling and Fracture of Steel Braces. *Journal of Structural Engineering,* 135**,** 19-32.

Kato, B. & Akiyama, H. (1973) Predictable propertier of material under incremental cyclic loading. *IABS, Preliminary publication***,** 119-124.

Martinez-Rueda, J. E. (2002) On the Evolution of Energy Dissipation Devices for Seismic Design. *Earthquake Spectra,* 18**,** 309-346.

Oliver-Saiz, E. & Benavent-Climent, A. (2011) Estudio numérico de la inestabilidad por pandeo de disipadores de energía tipo WPD. *4º Congreso Nacional de Ingenieria Sismica.*

Shanley, F. R. (1947) Inelastic Column Theory. *Journal of the Aeronautical Sciences* 14.

Symans, M. D., Charney, F. A., Whittaker, A. S., Constantinou, M. C., Kircher, C. A., Johnson, M. W. & Mcnamara, R. J. (2008) Energy Dissipation Systems for Seismic Applications: Current Practice and Recent Developments. *Journal of Structural Engineering,* 134**,** 3-21.

Tremblay, R. (2002) Inelastic seismic response of steel bracing members. *Journal of Constructional Steel Research,* 58**,** 665-701.

Xie, Q. (2005) State of the art of buckling-restrained braces in Asia. *Journal of Constructional Steel Research,* 61**,** 727-748.